

KEK-TH-1008
 KOBE-FHD-05-01
 HUPD-0501

The Decay of Tau Leptons Produced in Neutrino-Nucleon Scatterings

Mayumi Aoki¹, Kaoru Hagiwara^{1,2},
 Kentarou Mawatari^{3y}, and Hiroshi Yokoya^{4,5z}

¹Theory Group, KEK, Tsukuba 305-0801, JAPAN

²Department of Particle and Nuclear Physics,
 Graduate University for Advanced Studies, Tsukuba 305-0801, JAPAN

³Graduate School of Science and Technology, Kobe University,
 Nada, Kobe 657-8501, JAPAN

⁴Department of Physics, Hiroshima University,
 Higashi-Hiroshima 739-8526, JAPAN

⁵Radiation Laboratory, RIKEN, Wako 351-0198, JAPAN

Abstract

Energy and angular distributions of the decay products in the CERN-to-Gargamelle appearance experiments are studied for the decay modes $\tau^+ \rightarrow e^+ \nu_e$ and $\tau^+ \rightarrow \mu^+ \nu_\mu$. We find that the decay particle distributions in the laboratory frame are significantly affected by the polarization. Rather strong azimuthal asymmetry of τ^+ and τ^- about the momentum axis is predicted, which may have observable consequences even at small statistics experiments.

E-mail address: mayumi.aoki@kek.jp

^yE-mail address: mawatari@radix.h.kobe-u.ac.jp

^zE-mail address: yokoya@theo.phys.sci.hiroshima-u.ac.jp

1 Introduction

Neutrino oscillation physics is one of the most attractive field of current particle physics, and plenty of theoretical and experimental studies are revealing the amazing nature of the neutrino sector, such as their non-zero masses and the large mixings. We are now entering the stage of precise determination of the mass-squared differences including their signs and the mixing angles. The CP phase of the MNS (Maki-Nakagawa-Sakata) lepton-flavor mixing matrix [1] also interests us.

On the other hand, it is also important to find the direct evidence of the neutrino oscillation within the three generations. It can be achieved by detecting appearance in the long baseline neutrino oscillation experiments with the initial beam. The CNGS (CERN Neutrino to Gran Sasso) long baseline experiments [2] with ICARUS [3] and OPERA [4] detectors aim to establish appearance by measuring the lepton production events caused by the charged current (CC) interactions. They are now under construction and plan to start taking data from the year 2006. It is also expected that the CNGS experiments will improve significantly the current upper limit on θ_{13} , which is the smallest of the three mixing angles in the three-flavor MNS matrix, by measuring $\bar{\nu}_e$ transition [5]. The CC events followed by the $\bar{\nu}_e$ decays contribute as background events to the signals of the $\bar{\nu}_e$ events. Thus, the detailed analysis of the CC events is important in the CNGS experiments.

Since the lepton has the large mass, $m = 1.78$ GeV, it immediately decays into several particles always including a neutrino (ν). For that reason, production will be detected through its decay particle distributions. On the other hand, the decay particle distributions from depend critically on its spin polarization. It is therefore important to consider the spin polarization of in addition to its production cross section.

Detailed discussions on the spin polarization of produced in neutrino-nucleon scattering can be found in the recent paper [6]. There, the quasi-elastic scattering (QE), the resonance production (RES) and the deep inelastic scattering (DIS) processes were considered for the production, and it was shown that the produced 's have high degree of polarization, and their spin direction depends non-trivially on the energy and the scattering angle of in the laboratory frame.

In this article, we study the decay distributions from leptons produced via the CC interactions, especially for the CNGS experiments. We consider the production in the neutrino-nucleon scattering and its subsequent decays, for the decay modes $\bar{\nu}_e \rightarrow \bar{\nu}_e \gamma$ and $\bar{\nu}_e \rightarrow \bar{\nu}_e \ell^+ \ell^-$ ($\ell = e, \mu$):

$$+ N \rightarrow \bar{\nu}_e + X; \quad \bar{\nu}_e \rightarrow \bar{\nu}_e \gamma \quad (1)$$

2 Tau production

Let us start with the brief summary of the cross section and spin polarization of produced via neutrino. One can find more details in Ref. [6].

2.1 Kinematics and the formalism

We consider production by the charged current (CC) reactions on a nucleon target:

$$(k) + N(p) \rightarrow (k^0) + X(p^0); \quad (2)$$

For the hadronic final states X , we consider three subprocesses; the quasi-elastic scattering (QE), the resonance production (RES) and the deep inelastic scattering (DIS) processes. The four-momenta are parametrized in the laboratory frame as

$$\begin{aligned} k &= (E; 0; 0; E); \\ p &= (M; 0; 0; 0); \\ k^0 &= (E; p \sin \theta; 0; p \cos \theta); \end{aligned} \quad (3)$$

and the following Lorentz invariant variables are introduced

$$Q^2 = q^2 = (k - k^0)^2; \quad (4)$$

$$W^2 = (p + q)^2; \quad (5)$$

Each subprocess is distinguished by the hadronic invariant mass W : $W = M$ for QE, $M + m < W < W_{cut}$ for RES. W_{cut} is an artificial boundary, and we regard that DIS process occurs in the regions of $W > W_{cut}^1$. We take $W_{cut} = 1.4$ GeV in this report.

The differential cross section and the spin polarization vector of produced X are obtained in the laboratory frame as [6]

$$\begin{aligned} \frac{d}{dE} \frac{d}{d\cos \theta} &= \frac{G_F^2}{2} \frac{p}{M} \left[2W_1 + \frac{m^2}{M^2} W_4 (E - p \cos \theta) + W_2 (E + p \cos \theta) \right. \\ &\quad \left. + \frac{W_3}{M} (E E + p^2) (E + E) p \cos \theta - \frac{m^2}{M} W_5 \right] \\ &\quad \frac{G_F^2}{2} \frac{p}{M} F; \end{aligned} \quad (6)$$

and

$$s_x = \frac{m \sin \theta}{2} (2W_1 - W_2 + \frac{E}{M} W_3 - \frac{m^2}{M^2} W_4 + \frac{E}{M} W_5) F; \quad (7a)$$

$$s_y = 0; \quad (7b)$$

$$\begin{aligned} s_z &= \frac{1}{2} (2W_1 - \frac{m^2}{M^2} W_4 (p - E \cos \theta) + W_2 (p + E \cos \theta) \\ &\quad + \frac{W_3}{M} (E + E) p (E E + p^2) \cos \theta - \frac{m^2}{M} W_5 \cos \theta) F; \end{aligned} \quad (7c)$$

where G_F is the Fermi constant and $F = M_W^2 = (Q^2 + M_W^2)$. $\mathbf{s} = (s_x; s_y; s_z)$ is defined in the rest frame in which the z -axis is taken along its momentum direction and the y -axis is along $k - k^0$, the normal of the scattering plane, in the laboratory frame. It is normalized

¹More detailed studies on π^0 productions via the CC reactions have recently been reported in Ref. [7].

as $\delta_{\mu\nu} = 1=2$ for pure spin eigenstates. $W_{i=1,\dots,5}$ are structure functions defined with the generic decomposition of the hadronic tensor,

$$W(p; q) = g W_1(p - q; \vec{Q}^2) + \frac{p \cdot p}{M^2} W_2(p - q; \vec{Q}^2) + i \frac{p \cdot q}{2M^2} W_3(p - q; \vec{Q}^2) + \frac{q \cdot q}{M^2} W_4(p - q; \vec{Q}^2) + \frac{p \cdot q + q \cdot p}{2M^2} W_5(p - q; \vec{Q}^2); \quad (8)$$

where the totally antisymmetric tensor is defined as $\epsilon_{0123} = 1$. These functions can be estimated for each process, QE, RES, and DIS, as follows.

2.2 Hadronic tensor

2.2.1 Quasi-elastic scattering (QE)

The hadronic tensor for the QE process, $n + p \rightarrow n + p$, is written by using the hadronic weak transition current J as follows [8]:

$$W^{QE} = \frac{\cos^2 c}{4} \sum_{\text{spins}} J \cdot J \cdot (W^2 - M^2); \quad (9)$$

where c is the Cabibbo angle. J is defined as

$$J = \bar{h}_p(p^0) \hat{j}^\mu \gamma_\mu(p) i = u_p(p^0) \bar{u}_n(p); \quad (10)$$

where is written in terms of the six weak form factors of the nucleon, $F_{1,2,3}^V$, F_A , F_3^A and F_p , as

$$= F_1^V + \frac{i}{2M} \frac{q}{q^2} F_2^V + \frac{q}{M} F_3^V + F_A + \frac{(p + p^0)}{M} F_3^A + \frac{q}{M} F_p \quad (11)$$

We can drop F_3^V and F_3^A because of the time reversal invariance and the isospin symmetry. Moreover, the vector form factors F_1^V and F_2^V are related to the electromagnetic form factors of nucleons under the conserved vector current (CVC) hypothesis:

$$F_1^V(q^2) = \frac{G_E^V - \frac{q^2}{4M^2} G_M^V}{1 - \frac{q^2}{4M^2}}; \quad F_2^V(q^2) = \frac{G_M^V - G_E^V}{1 - \frac{q^2}{4M^2}}; \quad (12)$$

where

$$G_E^V(q^2) = \frac{G_M^V(q^2)}{1 + \frac{1}{(1 - \frac{q^2}{M_V^2})^2}} \quad (13)$$

with a vector mass $M_V = 0.84$ GeV and $= 3.706$. For the axial-vector form factor F_A and the pseudoscalar form factor F_p , we use

$$F_A(q^2) = \frac{F_A(0)}{(1 - \frac{q^2}{M_A^2})^2}; \quad F_p(q^2) = \frac{2M^2}{m^2 - q^2} F_A(q^2); \quad (14)$$

with $F_A(0) = 1.27$ [9] and an axial-vector mass $M_A = 1.026$ GeV [10]. Notice that the pseudoscalar form factor F_p plays an important role for the polarization of produced by neutrino because its contribution is proportional to the lepton mass and it has the spin-1/2 nature, although it is not known well experimentally; see Ref. [11] for details.

2.2.2 Resonance production (RES)

The hadronic tensor for the resonance production (RES) process, $+ n(p) \rightarrow + (p^+)$, is calculated in terms of the $N - \bar{N}$ weak transition current J as follows [8, 12, 13]:

$$W^{RES} = \frac{\cos^2 c}{4} \sum_{\text{spins}} J \bar{J} \frac{p \frac{W}{W(W)} =}{W^2 M^2 + iW(W)}^2 \quad (15)$$

with the running width

$$(W) = (M) \frac{M}{W} \frac{\frac{1}{2}(W^2; M^2; m^2)}{\frac{1}{2}(M^2; M^2; m^2)} : \quad (16)$$

$(M) = 0.12 \text{ GeV}$ and $(a; b; c) = a^2 + b^2 + c^2 - 2(ab + bc + ca)$. The current J for the process $+ n \rightarrow +$ is parametrized as

$$J = h^+(p^0) \bar{j}^+ j(p) i = (p^0) u_n(p); \quad (17)$$

where h is the spin-3/2 particle wave function and the vertex is expressed in terms of the eight weak form factors $C_{i=3,4,5,6}^{V,A}$ as

$$= \frac{g \bar{q} q}{M} C_3^V + \frac{g p^0 q \bar{p} q}{M^2} C_4^V + \frac{g p q \bar{p} q}{M^2} C_5^V + \frac{q \bar{q}}{M^2} C_6^V \quad 5 \\ + \frac{g \bar{q} q}{M} C_3^A + \frac{g p^0 q \bar{p} q}{M^2} C_4^A + g C_5^A + \frac{q \bar{q}}{M^2} C_6^A : \quad (18)$$

By using the isospin invariance and the Wigner-Eckart theorem, we obtain another $N - \bar{N}$ weak transition current as $h^+ \bar{j}^+ j(p) = \bar{3}h^+ \bar{j}^+ j(p)$. From the CVC hypothesis, $C_6^V = 0$ and the other vector form factors $C_{i=3,4,5}^V$ are related to the electromagnetic form factors. Assuming the magnetic dipole dominance [14], we have $C_5^V = 0$ and $C_4^V = \frac{M}{M} C_3^V$. For C_3^V , we adopt the modified dipole parametrizations [15, 16]:

$$C_3^V(q^2) = \frac{C_3^V(0)}{1 - \frac{q^2}{M_V^2}} \frac{1}{1 - \frac{q^2}{4M_V^2}} \quad (19)$$

with $C_3^V(0) = 2.05$ and $M_V = 0.735 \text{ GeV}$. For the axial form factors, we use [15]

$$C_5^A(q^2) = \frac{C_5^A(0)}{(1 - \frac{q^2}{M_A^2})^2} \frac{1}{1 - \frac{q^2}{3M_A^2}}; \quad C_6^A(q^2) = \frac{M^2}{m^2} \frac{C_5^A(q^2)}{q^2}; \quad (20)$$

with $C_5^A(0) = 1.2$ and $M_A = 1.0 \text{ GeV}$. For C_3^A and C_4^A , $C_3^A = 0$ and $C_4^A = \frac{1}{4}C_5^A$ give good agreements with the data [12]. As in the case of $F_p(q^2)$ in the QE process, the pseudoscalar form factor $C_6^A(q^2)$ has significant effects on the production cross section and the polarization [11].

2.2.3 Deep inelastic scattering (DIS)

In the DIS region, the hadronic tensor is estimated by using the quark-parton model:

$$W^{DIS}(p; q) = \sum_{q\bar{q}}^X \frac{d}{x} f_{q\bar{q}}(x; Q^2) K^{(q\bar{q})}(p_q; q); \quad (21)$$

where $p_q = p$ is the four-momentum of the scattering quark, x is its momentum fraction, and $f_{q\bar{q}}$ are parton distribution functions (PDFs) inside a nucleon. The quark tensor $K^{(q\bar{q})}$ is

$$K^{(q\bar{q})}(p_q; q) = (2 p_q \cdot q \cdot Q^2 / m_{q^0}^2) [2 g(p_q \cdot q) + 2 p_q p_{q^0} + p_q q + q p_{q^0} + i p_{q^0} q]; \quad (22)$$

The upper sign should be taken for quarks and the lower sign for antiquarks. We retain the val quark mass m_{q^0} for the charm quark as $m_c = 1.25$ GeV, but otherwise we set $m_{q^0} = 0$. In the calculation, we used MSTW 2002 [17] for the PDFs².

By neglecting both the nucleon mass and the initial quark masses, the following relations are obtained:

$$W_1(p \cdot q; Q^2) = F_1(x; Q^2); \quad W_{i=2, \dots, 5}(p \cdot q; Q^2) = \frac{M^2}{p \cdot q} F_{i=2, \dots, 5}(x; Q^2); \quad (23)$$

Here,

$$F_1 = \sum_{q\bar{q}}^X f_{q\bar{q}}(x; Q^2); \quad F_2 = 2 \sum_{q\bar{q}}^X f_{q\bar{q}}(x; Q^2);$$

$$F_3 = 2 \sum_q^X f_q(x; Q^2); \quad F_4 = 0; \quad F_5 = 2 \sum_{q\bar{q}}^X f_{q\bar{q}}(x; Q^2); \quad (24)$$

where $x = Q^2 = 2p \cdot q$ for massless val quarks ($m_{q^0} = 0$), and $x = x = w$ with $w = Q^2 = (Q^2 + m_{q^0}^2)$ for $q^0 = c$. In fact, the differential cross section, Eq. (6), does not satisfy the positivity condition near the threshold with this naive replacement. We modify the W_1 structure function as $W_1 = (1 + \frac{M^2}{p \cdot q}) F_1$ in order to preserve the positivity [6].

2.3 Polarization of produced at a fixed neutrino energy

We summarize the cross section and spin polarization of produced in neutrino-nucleon scattering for isoscalar targets at the incident neutrino energy $E = 10$ GeV on the $p \cos \theta - p \sin \theta$ plane, where p and θ are the momentum and the scattering angle in the laboratory frame.

In Fig. 1, the differential cross sections $d = dp_z dp_T$, obtained by transformation of variables in Eq. (6), are described as a contour map³, where $p_z = p \cos \theta$ and $p_T = p \sin \theta$. Only the contours of the DIS cross section are plotted to avoid too much complexity. The

²We adopt a naive extrapolation of the parton model calculation for low Q^2 in the $W > W_{cut}$ region, by freezing the PDFs when $Q^2 < Q_0^2 (= 1.25$ GeV²).

³It must be noted that this contour map differs from Fig. 11 of Ref. [6], where $d = dE / d \cos \theta$ is plotted.

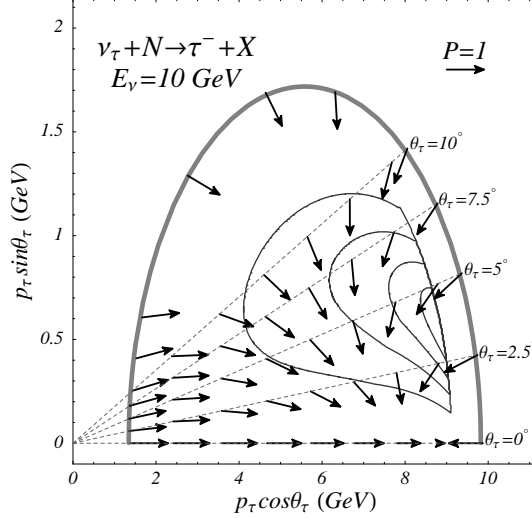


Fig. 1: The contour map of the D IS cross section on the $p_{\tau} \cos \theta_{\tau}$ - $p_{\tau} \sin \theta_{\tau}$ plane for the $\nu_{\tau} + N \rightarrow \tau^- + X$ process at $E_{\nu} = 10 \text{ GeV}$ in the laboratory frame. The kinematical boundary is shown by the thick curve. The QE process contributes along the boundary, and the RES process contributes just inside of the boundary. The polarization are shown by the arrows. The length of the arrows give the degree of polarization, and the direction of arrows give that of the spin in the rest frame. The size of the 100% polarization ($P = 1$) arrow is shown as a reference. The arrows are shown along the laboratory scattering angles, $\theta_{\tau} = 0, 2.5, 5, 7.5$, and 10 , as well as along the kinematical boundary.

kinematical boundary is shown by the thick curve. The QE process contributes along the boundary, and the RES process contributes just inside of the boundary. The contour map shows that the contributions in the forward scattering angles in the larger p_{τ} side are important. In that region, the cross sections of QE and RES are also large and comparable to that of D IS, where the highest of the contour corresponds to 0.004 pb/GeV^2 .

The polarization vector s , Eq. (7), of is also shown in Fig. 1. The length of each arrow gives the degree of polarization ($0 \leq P \leq 1$) at each kinematical point and its orientation gives the spin direction in the rest frame. The produced have high degree of polarization, but their spin directions significantly deviate from the massless limit predictions, where all should be purely left-handed. Since s_x of Eq. (7) turns out to be always negative, the spin vector points to the direction of the initial neutrino momentum axis. Qualitative feature of this results have been understood by considering the helicity amplitudes in the center of mass (CM) frame of the scattering particles and the effects of Lorentz boost from the CM frame to the laboratory frame. See more details in Ref. [6]. Let us stress that these features of the polarization of play an important role in the following analysis.

2.4 Polarization of produced in the CNGS experiments

In the CNGS experiments, beam is produced at CERN-PS, which is expected to deliver 4.5×10^{19} protons on target (p.o.t.) per year. The beam is optimized for appearance

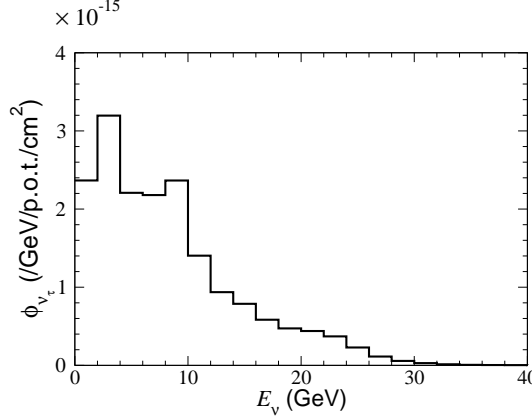


Fig. 2: The incoming flux with the three-neutrino model in the CNGS experiments. The neutrino oscillation probabilities are calculated for a set of parameters: $m_{12}^2 = 8.2 \times 10^{-5} \text{ eV}^2$ and $m_{13}^2 = 2.5 \times 10^{-3} \text{ eV}^2$, $\sin^2 2_{12;23;13} = 0.8; 1; 0$, respectively, the CP phase $\text{M}_{\text{NS}} = 0$, and the matter density $= 3 \text{ g/cm}^3$.

with a mean neutrino energy of about 17 GeV. Fig. 2 shows the expected flux

$$\langle E \rangle = \sum_{\nu} \langle E_{\nu} \rangle P_{\nu \rightarrow \text{e}} \quad (25)$$

at Gran Sasso with the baseline length of $L = 732 \text{ km}$ from CERN. Here $\langle E \rangle$ are the initial fluxes ($\nu = e$; ν) [2] and $P_{\nu \rightarrow \text{e}}$ are the oscillation probabilities in the three-neutrino model. The fraction $e =$ in the initial fluxes is less than 1%. The neutrino oscillation probabilities are calculated for a set of the three neutrino model parameters: two mass-squared differences $m_{12;13}^2$, three mixing angles $12;23;13$ and the CP phase M_{NS} in the MNS matrix [1], and the matter density $.$ The CHOOZ [8] and Palo Verde [19] reactor experiments give the upper bounds on $\sin^2 2_{13}$, as $\sin^2 2_{13} < 0.16$ for $m_{13}^2 = 2.5 \times 10^{-3} \text{ eV}^2$. The values of m_{12}^2 and $\sin^2 2_{12}$ are constrained by the observations of the solar neutrinos [20] and the KamLAND experiment [21], and those of m_{13}^2 and $\sin^2 2_{23}$ by the atmospheric neutrino observation at Super-Kamiokande [22] and the K2K experiment [23]. No constraint on the CP phase has been given by the present neutrino experiments. In our analysis, we take the following values for the neutrino oscillation parameters:

$$m_{12}^2 = 8.2 \times 10^{-5} \text{ eV}^2; \quad m_{13}^2 = 2.5 \times 10^{-3} \text{ eV}^2; \\ \sin^2 2_{12} = 0.8; \quad \sin^2 2_{23} = 1; \quad \sin^2 2_{13} = 0; \quad \text{M}_{\text{NS}} = 0; \quad (26)$$

with the constant matter density of $= 3 \text{ g/cm}^3$. Here we assume the so-called normal hierarchy. Because of setting $\sin^2 2_{13} = 0$, the neutrino oscillation probabilities are approximately described by those in the two neutrino (ν and $\bar{\nu}$) model. See e.g., Ref. [24] for details.

Taking into account the CNGS neutrino flux shown in Fig. 2, we show the distributions of events and polarization vectors of ν on the $p \cos \theta - p \sin \theta$ plane in Fig. 3. The right figure is an enlargement of the left figure to show the polarization vectors in detail for the important region of large cross section. The initial neutrino energy is integrated out

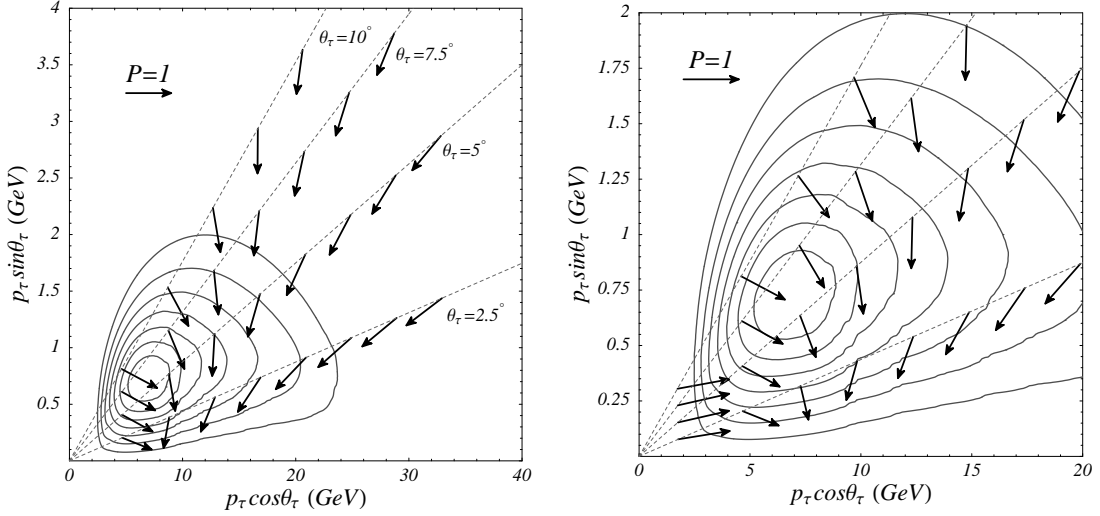


Fig. 3: The contour map of the number of production events on the $p_{\tau} \cos \theta_{\tau}$ - $p_{\tau} \sin \theta_{\tau}$ plane in the CNGS experiments. The polarization are shown by the arrows. The length of the arrows give the degree of polarization, and the direction of arrows give that of the spin in the rest frame. The size of the 100% polarization ($P = 1$) arrow is shown as a reference. The arrows are shown along the laboratory scattering angles, $\theta_{\tau} = 2.5^\circ, 5^\circ, 7.5^\circ$, and 10° . The right figure is an enlargement of the left figure.

with the incoming flux, $\langle E \rangle$ of Eq. (25), whereas it is fixed at 10 GeV in Fig. 1. The number of production events for all the QE, RES and DIS processes are included in the contour map, where we assume 5 years with 4.5×10^{19} p.o.t./year of the primary proton beam and the 1.65 kton size detector, which are the current plan of the OPERA experiment [4]. Each contour line gives a number of events per GeV^2 . For example, the highest contour line corresponds to 7 events/ GeV^2 . The contour map shows that there are many events around $E = 10 \text{ GeV}$, and around $\theta_{\tau} = 5^\circ$. As for the polarization vectors, the dependence on the energy and the scattering angle of τ is rather smooth as compared to that in Fig. 1 because of the integration of the incident neutrino energy. As the right figure shows, however, the direction of the polarization is still non-trivial in the region which has many events.

3 Tau decay

3.1 Tau decay in the rest frame

Before turning to the decay in the CNGS experiments, we give the formulas of the energy and angular distributions of the decay particles, especially τ and ν , from the polarized lepton in the rest frame. The decay distributions in the laboratory frame can be easily obtained by simple Lorentz transformation. Here again we note that the z-axis of the rest frame, in which we calculate the spin polarization vector of τ , is taken along its momentum direction in the laboratory frame.

The decay distribution of ν via the decay mode $\nu \rightarrow \nu + \gamma$ is given as

$$\frac{1}{\Gamma} \frac{d\Gamma}{dE \cdot d\hat{\Omega}} = B \cdot \frac{1}{4} \cdot \frac{1}{1 + \frac{2\hat{s} \cdot \hat{p}}{p^2}} \cdot \frac{1}{E^2 - (m^2 + m^2) + 2m} ; \quad (27)$$

where Γ is the total decay width of ν and $B = B(\nu \rightarrow \nu + \gamma) = 11.06\%$ [9] is the decay branching fraction. All the frame dependent variables with hat (^) symbols are those in the rest frame. The energy of ν is fixed as $E = (m^2 + m^2)^{1/2}$, because of the 2-body decay kinematics. The angular distribution of γ is dictated by the γ polarization, and γ prefers to be emitted along the polarization direction.

Similarly, the decay distribution of ν via the decay mode $\nu \rightarrow \nu + e^- + \nu$ ($e^- = e$; $\nu = \bar{\nu}$) is given as

$$\frac{1}{\Gamma} \frac{d\Gamma}{dE \cdot d\hat{\Omega}} = B \cdot \frac{1}{4} \frac{2}{E_{\max}^4 f(m^2 - m^2)} \cdot \frac{1}{p \cdot E \cdot 3E_{\max}^2 - 2E^2 - \frac{m^2}{E^2} + \frac{2\hat{s} \cdot \hat{p}}{p^2} \frac{\hat{p} \cdot \hat{p}}{E^2} - E_{\max}^2 - 2E^2 + \frac{m^2}{m}} ; \quad (28)$$

where $E_{\max} = (m^2 + m^2)^{1/2} = 2m$ and the branching fraction of $\nu \rightarrow \nu + e^- + \nu$, B , is 17.84% for $e^- = e$ and 17.37% for $e^- = \bar{\nu}$ [9]. The normalization function is $f(y) = (1 - 8y + 8y^3 - y^4 - 12y^2 \ln y)^{-1/2} = (1 + y)^{-1/2}$. The distribution of γ depends on its energy, and has a peak in the high energy. Furthermore, the high energy γ tends to be emitted against the direction of the spin, although the impact is smaller than that of the ν case. It is meaningful to notice that, therefore, ν and $\bar{\nu}$ tend to have the opposite preference of the spin dependence on their angular distribution.

3.2 Tau decay in the CNGS experiments

In this section, we present our results of the decay particle distributions from leptons produced by the CC interactions for the CNGS experiments. Main feature of our analysis is to deal with the proper spin polarization of ν which is calculated for each production phase space, shown in Fig. 3. In order to show the effects of the polarization on the decay distributions, we compare the results with unpolarized decays and also with completely left-handed decays.

The events of the decay distributions for $i = \nu, \bar{\nu}$ are given by

$$\frac{dN_i}{dE_i d\Omega_i} = A \frac{Z_{E_{\max}}}{E_{\text{thr}}} \frac{dE}{dE} \frac{Z_1}{c_{\text{min}}} \frac{d\cos\theta}{dE} \frac{Z_{E_+}}{E_+} \frac{d}{dE} \frac{d\cos\theta}{dE} (E) \frac{1}{dE_i d\Omega_i} (E; \theta; s(E; E; \theta)) ; \quad (29)$$

where A is the number of active targets, E_{\max} is the maximum value of neutrino energy in the flux, $E_{\text{thr}} = m + m^2/2M$ is the threshold energy to produce lepton on a nucleon, and the other integral ranges are given by

$$c_{\text{min}}(E) = \frac{p}{1 + M} = E + M^2 - E^2 - m^2 = 4E^2 - M^2 = m^2 ;$$

$$E_-(E; \theta) = (b - \frac{b^2 - ac}{2}) = a ;$$

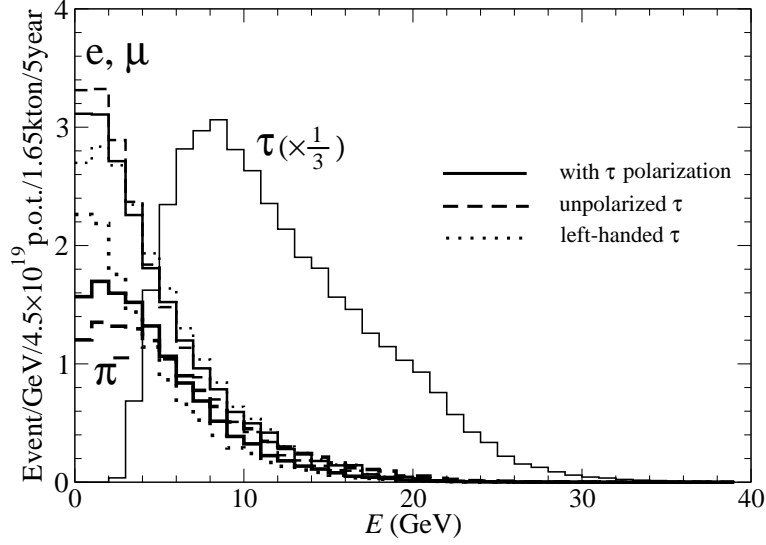


Fig. 4: Energy distributions of τ (thick lines) and π ($= e$; μ) (medium-thick lines) in the decay of τ produced in the neutrino-nucleon CC interactions for the CNGS experiments. 5 years running with 4.5×10^{19} p.o.t./year of the primary proton beam and 1.65 kton detector are assumed. Solid, dashed, and dotted lines show the energy distributions with the predicted polarization, unpolarized, and purely left-handed cases, respectively. The estimated number of τ production is also shown by a thin solid line with respect to the energy (E).

where $a = (E + M)^2 - E^2 \cos^2 \theta$, $b = (E + M)(M E + m^2 = 2)$, $c = m^2 E^2 \cos^2 \theta + (M E + m^2 = 2)^2$. Here, all the frame dependent variables are defined in the laboratory frame. E and θ dependence of $d\tau = dE d\theta$ appear by the Lorentz transformation from the rest frame to the laboratory frame. Although we retain only the e or μ momenta in the above formula, more exclusive measurements may be possible. For example, a well-developed emulsion detector used in OPERA experiment [4] can detect the kink of decay and can measure the scattering angle of τ with the accuracy of π rad, and also the flight length is measurable. Therefore it would be possible to do more detailed analysis of events, if there were enough statistics.

Fig. 4 shows the energy distributions of τ (thick lines) and π ($= e$; μ) (medium-thick lines) decayed from τ produced in the neutrino-nucleon CC interactions. We assume the same configuration of the experimental setup as Fig. 3, i.e., 5 years running with 4.5×10^{19} p.o.t. per year of the primary proton beam and 1.65 kton size detector for the OPERA experiment [4]. (For the ICARUS experiment, 2.35 kton of liquid Argon detector mass and 10 years running are planned [3], so that more statistics are expected.) For each decay mode, solid lines show the distributions from the decay of τ with the predicted polarization. For comparison, dashed and dotted lines show those of unpolarized and purely left-handed τ , respectively. The estimated number of the τ production with respect to the lepton energy, E , is also plotted as a thin solid line. The results are calculated by using Eq. (29) with 100% particle detection efficiency for simplicity. For the above parameters, 113 events of τ are produced and 13 (20) of those decay into (π) mode.

The τ and π distributions have peak in the low energy region, and in this region

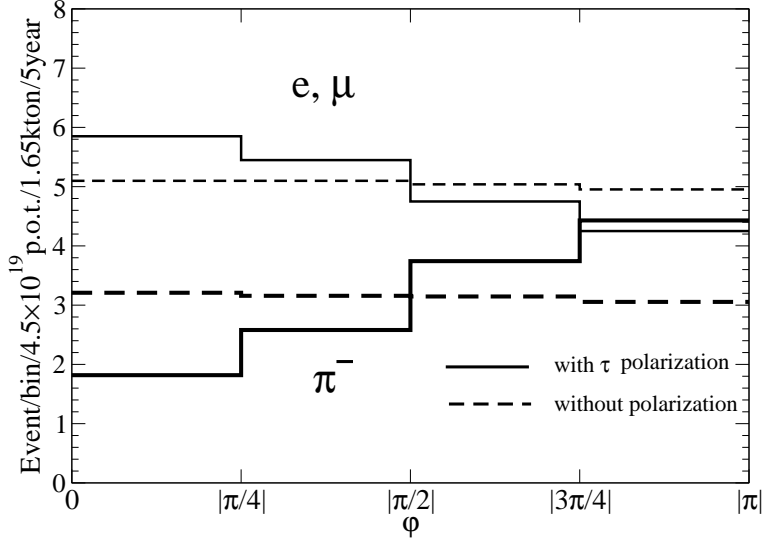


Fig. 5: A azimuthal angle distribution of (thick lines) and (thin lines). The configurations, such as neutrino flux, detector size etc., are the same as Fig. 4. Solid lines show the distributions from with the predicted polarization, and dashed lines show those with the unpolarized case. The results of purely left-handed are the same as those for the unpolarized .

the polarization dependence becomes large. As we pointed out in the previous section, the polarization dependence is opposite between and , and is more significant in

than in . In the peak region, the polarization dependence affects the distribution around 30% (15%) for the () decay mode. Expected statistics is rather small in the current design of the CNGS experiments. However, the likelihood probability of each event will be affected significantly by the polarization effects. The characteristic feature of our prediction is that the produced is almost fully polarized and that it has non-zero transverse component of the spin vector, namely s_x of Eq. (7). The observed patterns of the and energy distributions in the laboratory frame then follow from the energy angular distributions in the polarized rest frame⁴.

Fig. 5 shows the azimuthal angle distribution of (thick lines) and (thin lines). The azimuthal angle is given by $d_i = d \cos \phi_i$ in Eq. (29), and is measured from the scattering plane where $\phi_i = \pi/2$ is along the p_\perp direction in the laboratory frame, in which the z-axis is taken along the direction of the momentum . Solid lines show the distributions from with the predicted polarization, and dashed lines show those from unpolarized . The results of purely left-handed are the same as those for the unpolarized . Since both unpolarized and purely left-handed have zero component of perpendicular polarization, they give flat azimuthal distributions. The azimuthal angle distributions can be measured by tracking the trajectory of leptons by emulsion detectors in the OPERA experiment, or by reconstructing the hadronic cascades from neutrino-nucleon scattering. As is the case of energy distribution, and decay mode show the opposite feature and polarization dependence is clearer on mode than mode. At $\phi = 0$ or π the dependence of the polarization affects the distribution by about

⁴We may note that we checked all our results by using TAUOLA (the Monte Carlo program to simulate decays of leptons) [25].

47% (16%) for the ν_e decay. Even though the number of event is limited, it may be possible to obtain a hint of such large asymmetries.

Finally we comment on the contributions of the neutrino oscillation parameters to our results. The number of ν_e production is very sensitive to the value of m_{13}^2 . When we take Eq. (26) but $m_{13}^2 = 3 \times 10^{-3} \text{ eV}^2$, about 50 more events of ν_e are obtained. On the other hand, the produced ν_e decreases (about 10% maximum) for the larger (smaller) value of $\sin^2 2_{13}$ ($\sin^2 2_{23}$). However those parameters do not change much the impacts of the polarization on the energy and angular distributions of the decay products.

4 Conclusion

In this article, we have studied the effects of the spin polarization of ν_e produced in neutrino-nucleon scattering on the subsequent decay distributions. The calculation of the cross section and the spin polarization of ν_e production processes, QE, RES and DIS, were reviewed and the decay distributions of ν_e into e^- or ν_e ($= e^-$; ν_e) modes were considered. Taking into account the polarization of produced ν_e , we calculated the energy and azimuthal angle distributions of e^- and ν_e in the laboratory frame, for the experimental setup of the CNGS long baseline project, OPERA and ICARUS experiments.

We found that the decay particle distributions in the laboratory frame are significantly affected by the polarization. Rather strong azimuthal asymmetry of e^- and ν_e about the momentum axis is predicted, which may have observable consequences even at small statistics experiments.

Before closing, let us mention about the decay particle distribution from ν_e^+ , although there is no plan to use ν_e^+ beam in the CNGS experiments so far. In this case the strong azimuthal asymmetry predicted for the ν_e^+ decay is not expected because the transverse component of the ν_e^+ polarization is rather small, as shown in Fig. 12 of Ref. [6].

Acknowledgments

K.M. would like to thank T.Morii for encouragements and S.Aoki for valuable comments. H.Y. would like to thank J.Kodaira for encouragement and RIKEN BNL Research Center for helpful hospitality during his stay. The work of K.H. is partially supported by the core university exchange program of JSPS.

References

- [1] Z. Maki, M. Nakagawa, and S. Sakata, *Prog. Theor. Phys.* 28 (1962) 870.
- [2] CNGS project home page, <http://projcngs.web.cern.ch/>.
- [3] e.g. A. Rubbia, *Nucl. Phys. B (Proc. Suppl.)* 91 (2001) 223,
see also ICARUS Collaboration home page, <http://pcnometh4.cern.ch/>.
- [4] OPERA Collaboration home page, <http://operaweb.web.cern.ch/>.

[5] See e.g., V. Barger et al., *Phys. Rev. D* 65 (2002) 053016; P. Huber et al., *Phys. Rev. D* 70 (2004) 073014.

[6] K. Hagiwara, K. Mawatari, and H. Yokoya, *Nucl. Phys. B* 668 (2003) 364; Erratum – *ibid.* 701 (2004) 405.

[7] K.S. Kuzmin, V.V. Lyubushkin, V.A. Naumov, *Mod. Phys. Lett. A* 19 (2004) 2815; K.S. Kuzmin, Seminar at KEK on Feb. 15, 2005.

[8] C.H. Llewellyn Smith, *Phys. Rep.* 3 (1972) 261.

[9] Particle Data Group (S. Eidelman et al.), *Phys. Lett. B* 592 (2004) 1.

[10] V. Bernard, L. Bouadimiri, and U. Meissner, *J. Phys. G* 28 (2002) R1.

[11] K. Hagiwara, K. Mawatari, and H. Yokoya, *Phys. Lett. B* 591 (2004) 113.

[12] P.A. Schreiner and F. Von Hippel, *Nucl. Phys. B* 58 (1973) 333.

[13] S.K. Singh, M.J. Vicente Vacas, and E. Oset, *Phys. Lett. B* 416 (1998) 23.

[14] L.A. Alvarez-Ruso, S.K. Singh, and M.J. Vicente Vacas, *Phys. Rev. C* 57 (1998) 2693; and references therein.

[15] E.A. Paschos, J.Y. Yu, and M. Sakuda, *Phys. Rev. D* 69 (2004) 014013.

[16] M.G. Olsson, E.T. Ospowski, and E.H. Mousay, *Phys. Rev. D* 17 (1978) 2938.

[17] A.D. Martin et al., *Eur. Phys. J. C* 23 (2002) 73.

[18] The CHOOZ Collaboration (M. Apollonio et al.), *Eur. Phys. J. C* 27 (2003) 331.

[19] The Palo Verde Collaboration (F. Boehm et al.), *Phys. Rev. D* 64 (2001) 112001.

[20] B. Kayser, in *Review of Particle Physics*, *Phys. Lett. B* 592 (2004) 1, pp. 145{153, and references therein.

[21] The KamLAND Collaboration (T. Araki et al.), [hep-ex/0406035](https://arxiv.org/abs/hep-ex/0406035).

[22] The Super-Kamiokande Collaboration (Y. Ashie et al.), *Phys. Rev. Lett.* 93 (2004) 101801.

[23] The K2K collaboration (M.H. Ahn et al.), *Phys. Rev. Lett.* 90 (2003) 041801.

[24] M. Aoki et al., *Phys. Rev. D* 67 (2003) 093004; K. Hagiwara, *Nucl. Phys. B (Proc. Suppl.)* 137 (2004) 84.

[25] S. Jadach, Z. Was, R. Decker, and J.H. Kuhn, *Comput. Phys. Commun.* 76 (1993) 361.